A comparative study of continuous versus stop-and-go scanning in circular scanning photoacoustic tomography

Sharma, Arunima; Kalva, Sandeep Kumar; Pramanik, Manojit

2018

Sharma, A., Kalva, S. K., & Pramanik, M. (2019). A comparative study of continuous versus stop-and-go scanning in circular scanning photoacoustic tomography. IEEE Journal of Selected Topics in Quantum Electronics, 25(1), 7100409-. doi:10.1109/JSTQE.2018.2840320

https://hdl.handle.net/10356/89541

https://doi.org/10.1109/JSTQE.2018.2840320

A comparative study of continuous versus stop-and-go scanning in circular scanning photoacoustic tomography

Arunima Sharma, Sandeep Kumar Kalva, and Manojit Pramanik

***Abstract*— Photoacoustic tomography (PAT) is a non-invasive hybrid imaging modality providing high contrast and resolution in deep tissue imaging. In a typical PAT system, photoacoustic (PA) waves are recorded using an ultrasound transducer rotating around the sample. Being economical and easily available, single element transducer (SET) is commonly employed. For each laser pulse the SET collects one time-resolved PA signal, known as an A-line. Acquisition of A-lines in a circular scanning PAT system by an SET can be done in two ways - (1) Stop-and-go scan, and (2) Continuous scan. In this work, we compared the two types of scanning methods in terms of image quality, signal-to-noise ratio (SNR), spatial accuracy, resolution, and scan-time for phantoms and *in vivo* imaging. We found that the image quality, spatial accuracy, and SNR did not change in continuous scans, as compared to stop-and-go scans. However, there was a significant decrease in scan time in continuous scans. This improvement in scan time was 2-4 folds for lasers with low pulse repetition rate (10 Hz), and up to 7-12 folds for lasers with higher pulse repetition rate (7 kHz).**

***Index Terms*— Circular scanning geometry, continuous scanning, photoacoustic tomography, single-element ultrasound transducer, stop-and-go scanning.**

I. Introduction

PHOTOACOUSTIC imaging (PAI) is a non-invasive imaging modality which works on the principal of photoacoustic effect [1-9]. In this effect, chromophores present in a sample/body absorb light, resulting in a local temperature rise and generation of acoustic wave due to thermoelastic expansion. PAI is done by acquisition of these acoustic waves. Being a hybrid imaging modality, PAI provides high optical contrast and high ultrasonic resolution. These advantages give it an edge over other imaging modalities for various clinical and pre-clinical applications like brain imaging [10, 11], sentinel lymph node imaging [12, 13], breast imaging [14-16], hemoglobin concentration [17] etc. In a conventional photoacoustic tomography (PAT)/photoacoustic computed tomography (PACT) system, nanosecond laser pulses illuminate a target sample which produces photoacoustic (PA) waves. A wideband ultrasound transducer (UST) acquires the PA waves, which contain information about the structural and optical properties of the sample. For deep tissue imaging, circular scanning geometry in orthogonal mode is preferred [2, 18-20]. With each laser pulse irradiating the sample, a time resolved PA signal, known as an A-line, is recorded. Once these A-lines at various positions around the sample are collected, reconstruction algorithms are used to map the initial pressure rise and the cross-sectional image of the sample accordingly [21-26].

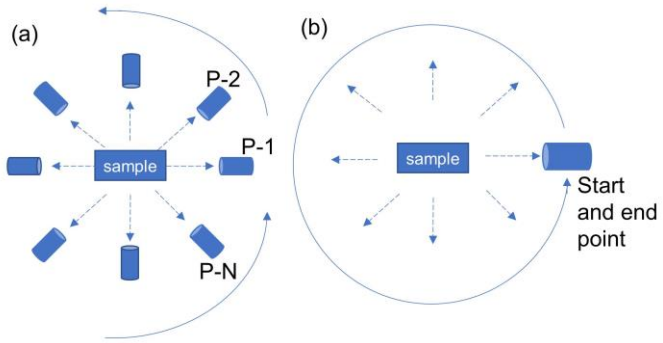

Fig. 1. Different types of scanning methods. (a) Stop-and-go scan: transducer stops at various positions (P) to collect the A-line. (b) Continuous scan: a moving transducer collects the A-lines and comes to a stop only after completing full rotation.

Various types of transducers can be used for signal acquisition in PAT/PACT. These include - single element transducer (SET) [27], linear array transducer [28-30], semi-circular array transducer [31], circular array transducer [32], or spherical array transducer [33]. Since SET-based systems can collect only one A-line per laser pulse, they have longer data acquisition time (scan-time) than PAT systems that use array transducers. Nevertheless, being economical, highly sensitive, and easily available, SETs are still used in PAT/PACT systems [34-36]. Reducing the scan time for SET-based systems remains a challenge. Use of lasers with high pulse repetition rate (PRR) reduces the scan time. As compared to traditional Nd:YAG laser, pulsed laser diode (PLD) and light emitting diode (LED) offer much higher PRR and therefore, use of these light sources in PAT/PACT system reduces the data acquisition time [37]. To further decrease the scan time, one can use continuous scan for data acquisition.

In SET-based systems, acquisition of PA signal can be done in two ways – 1) stop-and-go scan [38], or 2) continuous scan

Manuscript received November 15, 2017. This work was funded by the Singapore Ministry of Health's National Medical Research Council (NMRC/OFIRG/0005/2016: M4062012).

Arunima Sharma, Sandeep Kumar Kalva, and Manojit Pramanik are with the Nanyang Technological University, School of Chemical and Biomedical Engineering, 62 Nanyang Drive, 637459, Singapore (e-mail: arunima001@e.ntu.edu.sg; sandeepk002@e.ntu.edu.sg, Address of correspondence: phone: +65-6790-5835; fax: +65-6791-1761; e-mail: manojit@ ntu.edu.sg).

[27]. In former, a motor rotates the UST around the sample in steps of predefined length. After each step the motor stops and waits for the UST to collect the required number of A-lines, before moving to the next position. This process continues till the UST completes one full rotation (360 degree) around the sample. After this, the A-lines are averaged and later reconstructed to form the cross-sectional image. This contrasts with the continuous scan in which the stepper motor moves the UST continuously around the sample at a constant speed. Multiple A-lines are collected by the moving transducer which stops once it has completed the entire rotation. The A-lines are then averaged, if needed, and reconstructed. Fig. 1 shows a graphic representation explaining the difference between the two types of scans.

In this work, we have compared stop-and-go and continuous scanning methods for SET-based PAT systems for phantoms and *in vivo* imaging of rat brain. We have first shown theoretically that the blurring effects of collecting data from a moving transducer in continuous scans are minimal, whereas there is a noticeable improvement in scan time. For experimental validation, two types of lasers have been used – traditional pulsed Nd:YAG laser at a PRR of 10 Hz, and a pulsed laser diode at 7 kHz PRR. The experimental results show that the image quality of continuous scans is as good as stop-and-go scans. Further, there is a significant improvement in scan time for continuous scans as compared to the traditional stop-and-go scans.

II. Materials and Methods

A. Nd:YAG based PAT imaging system

The schematic of PAT system using Nd:YAG laser is shown in Fig. 2(a). A Q-switched Nd:YAG laser (Continuum, Surelite Ex) was used to deliver laser pulses of pulse-width 5 ns at a PRR of 10 Hz and wavelength of either 532 nm or 1064 nm. For phantom (point-source) imaging, a wavelength of 532 nm was used, whereas 1064 nm was used for animal imaging. The laser pulses were reflected towards the sample by using three right angled prisms (PS911, Thorlabs). An optical diffuser was used to homogenize the laser beam. The laser pulse fluence on the surface of sample was maintained at ~6 mJ/cm^2 for 532 nm wavelength, and ~25 mJ/cm^2 for 1064 nm wavelength. Both these values are within the ANSI safety limit, which is ~20 mJ/cm^2 at 532 nm and ~100 mJ/cm^2 at 1064 nm for a laser with PRR of 10 Hz [39].

For phantom imaging, signal was acquired using a cylindrically focused UST (Olympus NDT, V306-SU-NK, CF = 1.90 in.) of central frequency 2.25 MHz, whereas for animal imaging, an unfocused UST (Olympus NDT, V309-SU) of central frequency 5 MHz was used. Both the transducers had a 13 mm diameter active area and ~70% nominal bandwidth. A stepper motor (Lin Engineering, Silverpak 23C) was used to rotate the UST around the sample. The UST was placed in a water tank to enable better coupling of the ultrasound signal. Once acquired, the PA signal was amplified by ~45 dB and filtered by a pulse amplifier (Olympus-NDT, 5072PR) and then recorded using a data acquisition card (DAQ) (GaGe, compuscope 4227) inside a desktop (Intel xeon 3.7 GHz 64-bit processor, 16 GB RAM). All the data was collected at a sampling rate of 25 MS/s. A sync signal from the laser was used to synchronize the data acquisition and laser excitation.

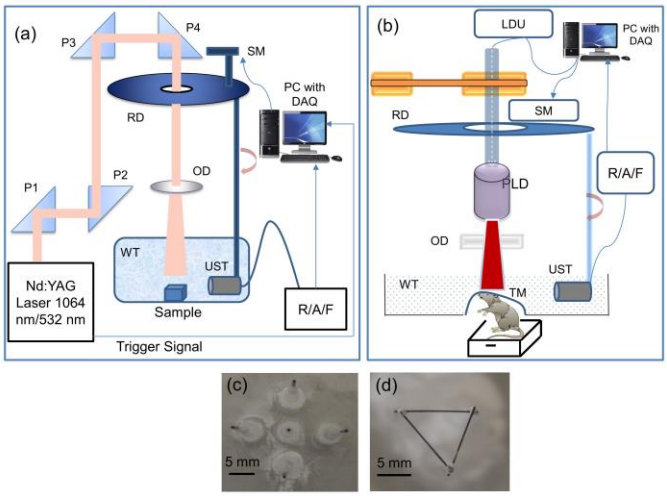

Fig. 2. Schematic for the PAT imaging systems using (a) Nd:YAG Laser and (b) Pulsed Laser Diode. RD: rotating disc, P1-P4: right-angled prisms, UST: ultrasound transducer, SM: stepper motor, PLD: pulsed laser diode, WT: water tank, OD: optical diffuser, LDU: laser driver unit, DAQ: Data acquisition card, R/A/F: receiver/amplifier/filter, TM: Transparent membrane. Photograph of (c) point source phantom, (d) triangle phantom.

B. PLD-based PAT imaging system

The schematic of PLD-PAT system is shown in Fig. 2(b). 136 ns pulse at ~803 nm wavelength was provided by the pulsed laser diode (Quantel, France). A laser driver unit (LDU) was used to manipulate the laser pulse. This LDU consisted of a temperature controller (LaridTech, MTTC1410), a 12V power supply (Voltcraft, PPS-11810), a variable power supply (BASETech, BT-153), and a function generator (FG250D, Funktions generator). The PLD generated ~1.4 mJ of energy (at a PRR of 7 kHz) per pulse, which passed through an optical diffuser (for uniform illumination) to illuminate ~16 cm^2 on the sample surface. Laser fluence on sample surface was ~0.05 mJ/cm^2. For a wavelength of 803 nm, the maximum permissible exposure (MPE) for an exposure of over 10 seconds is ~317 mW/cm^2 [39]. Thus, for a PRR of 7000 Hz, MPE is ~0.045 mJ/cm^2. The sync signal from the function generator synchronized the data acquisition and laser excitation. PA signal was acquired using a flat 2.25 MHz UST (Olympus NDT, V306-SU). The characteristics of UST, stepper motor, as well as DAQ were the same as those used for Nd:YAG based PAT system. Once collected, the A-lines were averaged and later delay-and-sum algorithm [22] was employed to reconstruct the cross-sectional PAT images.

C. Data acquisition

Continuous scans are generally faster than stop-and-go scans. If the angular velocity (ω) and the angular acceleration (α) are known for a motor which completes its rotation in N steps, time taken for it to move around the sample is given by

$$t_{rotation} = \frac{2\pi}{\omega} + \frac{N\omega}{\alpha}. \quad (1)$$

For continuous scans, N = 1 and no extra time is required for collection of A-lines. Therefore,

$$t_{continuous} = \frac{2\pi}{\omega} + \frac{\omega}{\alpha}. \quad (2)$$

If the same number of A-lines is to be collected for both types of scan method, total time taken for stop-and-go scan will be

$$t_{stop-and-go} = t_{continuous} + t_{rotation}. \quad (3)$$

For continuous scans, the time of rotation depends only upon the number of A-lines to be collected, whereas for stop-and-go scans, time can be varied by varying the number of steps, velocity, and acceleration of the motor, while keeping the number of A-lines collected constant. The time of rotation can be decreased by decreasing the number of steps, but that increases the angle between two consecutive positions where A-lines are collected, thereby deteriorating the image quality. Another method to decrease the scan time is by increasing the velocity and acceleration of the motor. However, this may result in increasing vibrations in the motor and therefore, is limited.

Although continuous scans are faster than stop-and-go scans, the latter are still preferred in some cases. For example, the blurring caused in continuous scans due to collection of A-lines by a fast-moving UST may be a deciding factor to choose stop-and-go scan. Nonetheless, it can be shown mathematically that the blur is inconsequential as compared to the resolution of PAT systems. If the sample diameter is d mm, and speed of sound in water 1.5 mm/μs, time taken for acoustic waves from the entire sample to reach the UST will be

$$t = \frac{d}{1.5}\mu s. \quad (4)$$

If the transducer completes one rotation in T seconds, angular displacement of the transducer while it collects acoustic waves from the furthest point of the sample is given by

$$\theta(radian) = \frac{2\pi}{T} \times \frac{d}{1.5} \times 10^{-6}. \quad (5)$$

During this time, the maximal displacement of sample with respect to transducer will be approximately,

$$\approx \frac{2\pi}{T} \times \frac{d}{1.5} \times 10^{-6} \times \frac{d}{2} mm. \quad (6)$$

Typically, the sample diameter is ~15 mm (say, small animal brain imaging), and the fastest scan time that has been reported so far is 3 seconds for completing one rotation [37]. Computing (6) using these values shows that the maximum displacement of the sample with respect to the transducer before it can record PA signal from across the sample, is ~0.15 μm, which is insignificant compared to the resolution of the PAT system (~182 μm with 5 MHz UST, and ~381 μm using 2.25 MHz UST [37]).

However, it should be noted that the pulse energy of nanosecond lasers fluctuates by about 20% between individual pulses. In stop-and-go scans, the fluctuation can be compensated for, by collecting multiple A-lines at the same point and averaging them. Moreover, averaging also helps in improving the signal-to-noise (SNR), which in turn improves the image quality. Averaging of signal for continuous scans is also possible, but motion of the UST results in relative motion of sample between two A-lines [40]. This relative distance depends on the speed of the UST and the PRR of the laser. For a UST, the relative displacement of sample between 2 A-lines, when the PRR of laser is *rep* Hz, will be

$$\approx \frac{2\pi}{T \times rep} \times \frac{d}{2} mm. \quad (7)$$

If we consider a PAT system wherein a sample of diameter 15 mm is imaged in 18 seconds, the distance moved by transducer between two A-lines for a 7 kHz laser will be 0.3 μm. If M A-lines are averaged together, the distance moved by the transducer becomes M fold. Therefore, for this system, if 500 A-lines are averaged, the relative displacement becomes 150 μm. Averaging is common while using lasers with high PRR like PLD and LED. The pulse energy of these lasers is usually low, which results in a low SNR of the image. Averaging is done to improve the SNR. Since the relative displacement of UST is inversely proportional to the PRR of laser, blurring caused due to this averaging is generally negligible. Nevertheless, blurring can result in a decline in image quality and therefore it should be taken care that the relative displacement remains within the limits of resolution even after averaging. For fair comparison, in this work, the averaging done for continuous scans is same as that done for stop-and-go scans.

In case of systems imaging larger objects, for example, breast imaging system, the sample diameter can be up to 15-20 cm [16, 41, 42]. Hence, there is an increase in both the relative displacement of UST while collecting signal from the sample, as well as the relative displacement of sample between collections of two consecutive A-lines. The effect of blurring due to continuous scan might be more prominent there. Thus, evaluation of speed at which the UST can rotate and the signal averaging that can be done becomes crucial and should be performed before choosing the optimum parameters for such imaging systems.

Another factor to be kept into account while doing a continuous scan is the Doppler effect. Due to relative motion of the sample and the UST, there is a shift in the detected ultrasound signal frequency. The frequency shift for an object moving at a velocity v relative to the detector (UST) at an angle θ is given by

$$\frac{\nabla f}{f} = \frac{v\cos\theta}{c} \approx \frac{2\pi}{T} \times \frac{d}{2} \times \frac{\cos\theta}{c}, \quad (8)$$

where, c is the speed of acoustic waves in medium (water). If we again consider the typical values of d = 15 mm, T = 3 seconds and c = 1.5 mm/μs, the maximum Doppler frequency shift would be ~0.001% (50 Hz for 5 MHz frequency component), and therefore is inconsequential and can be ignored [40].

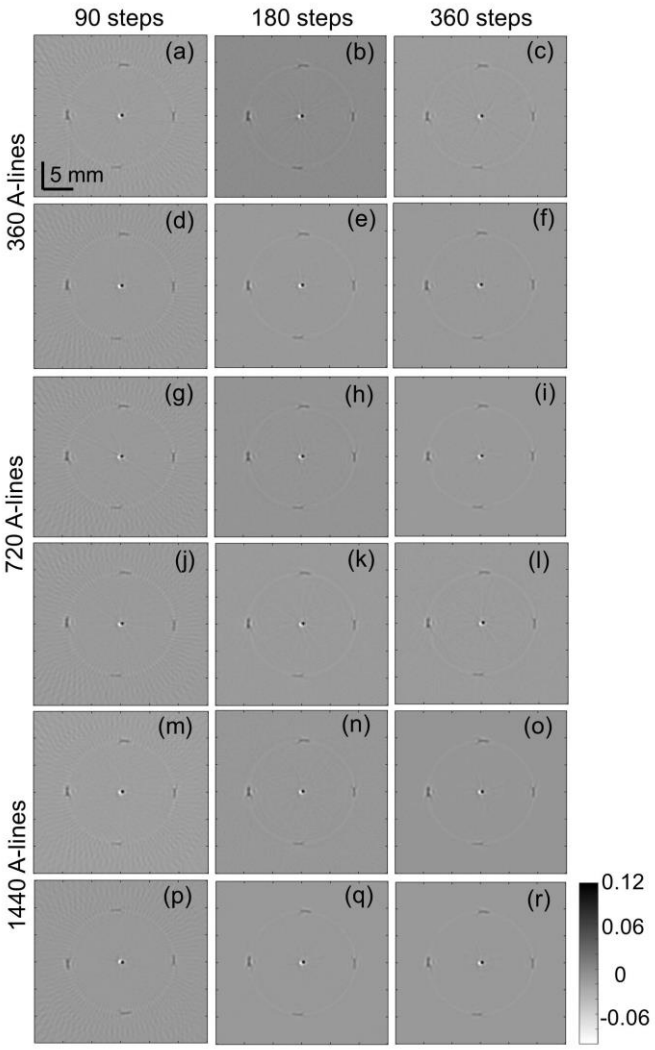

Fig. 3. Comparison of PAT images of point source phantom using (a-c, g-h, m-o) stop-and-go and (d-f, j-k, p-r) continuous scanning methods. (a-f) 360, (g-l) 720, and (m-r) 1440 A-lines were collected by moving the motor in (a, g, m) 90, (b, h, n) 180, and (c, l, o) 360 steps. The images obtained using continuous scans were averaged in (d, j, p) 90, (e, k, q) 180, and (f, l, r) 360 A-lines. Scale bar as shown in (a).

D. Phantom imaging

Two phantoms were used to compare the two scanning methods. A point source phantom was imaged using Nd:YAG based PAT system and a shape phantom was imaged using PLD-PAT system. The point source phantom was prepared using five pencil leads of diameter 0.5 mm. These leads were stuck inside pipette tubes which were fixed vertically on an acrylic slab. The pipette tubes were used to keep the leads stable and vertical [Fig. 2(c)]. One lead was placed at the scanning center and the other four were placed at ~1 cm distance in four different directions from the center lead. For comparison, 180, 360, 720, 1440, and 2880 A-lines were collected for both the types of scans. For stop-and-go scan, the step size was kept 1°, 2°, and 4° in different scans, and then the desired total number of A-lines was collected by changing the number of A-lines collected after each stop. For example, when total number of A-lines collected was 720, the UST collected 2 A-lines per step when step size was 1°, 4 A-lines per step when step size was 2°, and 8 A-lines per step when step size was 4°. To change the number of A-lines collected for continuous scan, the speed of the motor was changed. Since the PRR of laser was fixed at 10 Hz, collection of 180, 360, 720, 1440, and 2880 A-lines was done by rotating motor such that it completed one rotation in 18, 36, 72, 144, and 288 seconds, respectively. Before reconstruction, averaging of A-lines was done. For stop-and-go scans, averaging was in accordance with the step size of motor, such that, finally 360, 180, and 90 A-lines were reconstructed, respectively. For fair comparison, number of A-lines reconstructed for continuous scans was 360, 180, and 90 as well.

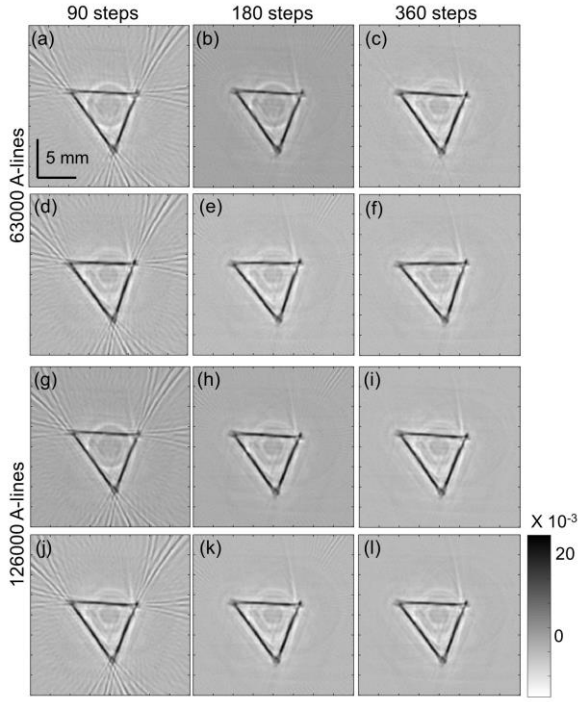

Fig. 4. PAT images for triangle sample for comparison of (a-c, g-i) stop-and-go and (d-f, j-l) continuous scanning methods. (a-f) 63000 and (g-l) 126000 A-lines were collected by scanning continuously for (d-f) 9 sec and (j-l) 18 sec and by scanning in (a, g) 90, (b, h) 180 and (c, i) 360 steps. The image was reconstructed by averaging the acquired A-lines in (a, d, g, j) 90, (b, e, h, k) 180, and (c, f, i, l) 360 A-lines. Scale bar as shown in (a).

Another phantom used for the experiments was a triangle made of horsehair of ~120 μm diameter. Three hairs of length ~1 cm were stuck with each other to form a triangle. This triangle was held using three pipette tips fastened on an acrylic slab. Fig. 2(d) shows a photograph of the triangle phantom. Images of triangle phantom were taken using PLD-PAT system. A-lines were collected by moving the UST around the sample in steps of 1°, 2°, and 4° (stop-and-go scans) and continuously for 9 and 18 seconds (continuous scans). Number of A-lines collected in 9 and 18 seconds were 63000 and 126000, respectively. Same numbers of A-lines were collected for different step sizes of stop-and-go scans as well. Averaging was done similar to the Nd:YAG-PAT system.

E. In vivo imaging

Healthy female rats weighing ~100 g were procured from

InVivos Pte. Ltd., Singapore and were used for conducting the *in vivo* imaging. Experiments were conducted in conformity with the approved guidelines and regulations by the institutional Animal Care and Use committee of Nanyang Technological University, Singapore (Animal Protocol Number ARF-SBS/NIE-A0263). The rats were anaesthetized using a combination of Ketamine (120 mg⁄kg) and Xylazine (16 mg⁄kg) injected intraperitoneally (dosage of 0.2 ml⁄100 g). Hair on the head of rat was epilated using hair removal lotion. A mixture of 1.0 L/min oxygen and 0.75% isoflurane was used to keep the rat anaesthetized during the experiment. The rat, along with its holder, was mounted on a translational stage which was used to adjust its height. The water tank was designed such that it had a hole in the center which was large enough to accommodate the rat's head. This hole was sealed using a clear, flexible membrane. The height of rat was adjusted such that its head protruded through the hole and was aligned in the same horizontal plane as the transducer. After scanning, the rat was euthanized by intraperitoneal injection of Valabarb (sodium pentobarbitone - 300 mg⁄ml).

III. Results and Discussion

A. Image quality

The reconstructed images of point source phantom are shown in Figs. 3(a-r). Reconstructed images obtained on collecting 360 A-lines, 720 A-lines, and 1440 A-lines are shown in Figs. 3(a-f), 3(g-l), 3(m-r), respectively. The reconstructed images of A-lines collected by employing stop-and-go scanning method are shown in Figs. 3(a-c), 3(g-i), 3(m-o) and those collected by using continuous scans are shown in Figs. 3(d-f), 3(j-l), 3(p-r). For both the types of scans, images formed on reconstruction of 90 [Figs. 3(a, d, g, j, m, p)], 180 [Figs. 3(b, e, h, k, n, q)], and 360 [Figs. 3(c, f, i, l, o, r)] A-lines are shown. It can be observed from the images that there is an improvement in image quality with an increase in number of steps (reconstructed A-lines), as expected. However, there is no difference in terms of visual image quality for both types of scanning methods.

Figs. 4(a-l) are the images of triangle phantom acquired after PLD-PAT scans. Figs. 4(a-f) and Figs. 4(g-l) were images obtained when 63000 A-lines and 126000 A-lines were collected, respectively. Before reconstruction, the A-lines were averaged according to the steps of stop-and-go scans. 90 A-lines were reconstructed in Figs. 4(a, d, g, j), 180 in Figs. 4(b, e, h, k), and 360 in Figs. 4(c, f, i, l). It was observed in these images that although the shape of phantom was retained, some artefacts were present in the background when the number of A-lines reconstructed was less. A noticeable decrease in artefacts was observed when the number of A-lines reconstructed increased from 90 to 180 and further to 360.

For both the phantoms, signal to noise ratio (SNR) was used to quantify the image quality. To compute SNR, the peak to peak amplitude of PA signal (V) was divided by the standard deviation of the background noise (n). Thus,

$$SNR = \frac{V}{n}, \tag{9}$$

A small region around the corner of the image, where there was no PA signal, was considered the background and n was computed using that area. V was calculated by taking an average of all the PA signals above a constant threshold value, in the area of interest. Table I shows the SNR of the different scans of point source phantom and triangle phantom. Several observations can be made from the table. Firstly, SNR increases with an increase in number of A-lines collected, provided the number of A-lines reconstructed is kept constant. This effect was up to 8% when the number of A-lines collected by Nd:YAG laser was doubled. However, no significant difference in SNR was observed in images obtained using PLD. Secondly, for a fixed number of A-lines collected, SNR value improved between 8% and 50% when the number of A-lines reconstructed increased from 90 to 360. Thirdly, if the number of A-lines collected and the number of A-lines reconstructed are kept the same, the SNR changed between 2-5% for stop-and-go scans and continuous scans.

For further comparison, the images obtained from different scans of point source phantom were evaluated for spatial accuracy. This was done by calculating the average distance of the center pencil lead from the other four leads. It was observed that the distance remained between 9.33 mm and 9.4 mm irrespective of the type of scan, number of A-lines collected, or the number of A-lines reconstructed. Repeating the experiments resulted in a change in distance of less than 0.6%. Therefore, it can be concluded that continuous scan does not affect the spatial accuracy of the system.

Following this, *in vivo* experiments were conducted using both Nd:YAG-PAT system as well as PLD-PAT system. The PAT images obtained are shown in Fig. 5 (using Nd:YAG laser), and in Fig. 6 (using PLD). While using Nd:YAG laser, 360, 720, and 1440 A-lines were collected. For continuous scans, this was achieved by moving the stepper motor at a velocity of 10°/second, 5°/second, and 2.5°/second, respectively. For stop-and-go scans, the velocity of motor was optimized at ~7°/second. Figs. 5(a-f), 5(g-l), and 5(m-r) show images obtained when 360, 720, and 1440 A-lines were collected, respectively. Among these, Figs. 5(a-c, g-i, m-o) were acquired using stop-and-go scans whereas Figs. 5(d-f, j-l, p-r) were acquired using continuous scans. Corresponding to the number of steps of stop-and-go scans, the A-lines of both stop-and-go and continuous scans were averaged to 90 A-lines [Figs. 5(a, d, g, j, m, p)], 180 A-lines [Figs. 5(b, e, h, k, n, q)], and 360 A-lines [Figs. 5(c, f, i, l, o, r)]. Photographs of the rat before and after skin removal are shown in Fig. 5(s) and Fig. 5(t), respectively.

SNR values for *in vivo* images are shown in Table II. An improvement in image quality and SNR was observed on increasing the number of collected A-lines, for both the types of scans. When the number of A-lines collected increased from 360 to 1440, SNR increased by ~27%. A similar increase in SNR was observed when the number of A-lines reconstructed

was increased from 90 to 360. Visually, the images appeared smoother and had lesser artefacts when more number of A-lines was collected and/or reconstructed. However, a maximum of just 7% change in SNR was observed between the images for stop-and-go scans and continuous scans when number of A-lines collected and reconstructed were kept constant. Moreover, there were instances when SNR of continuous scans was better than stop-and-go scans. Therefore, such changes in SNR values can be considered negligible.

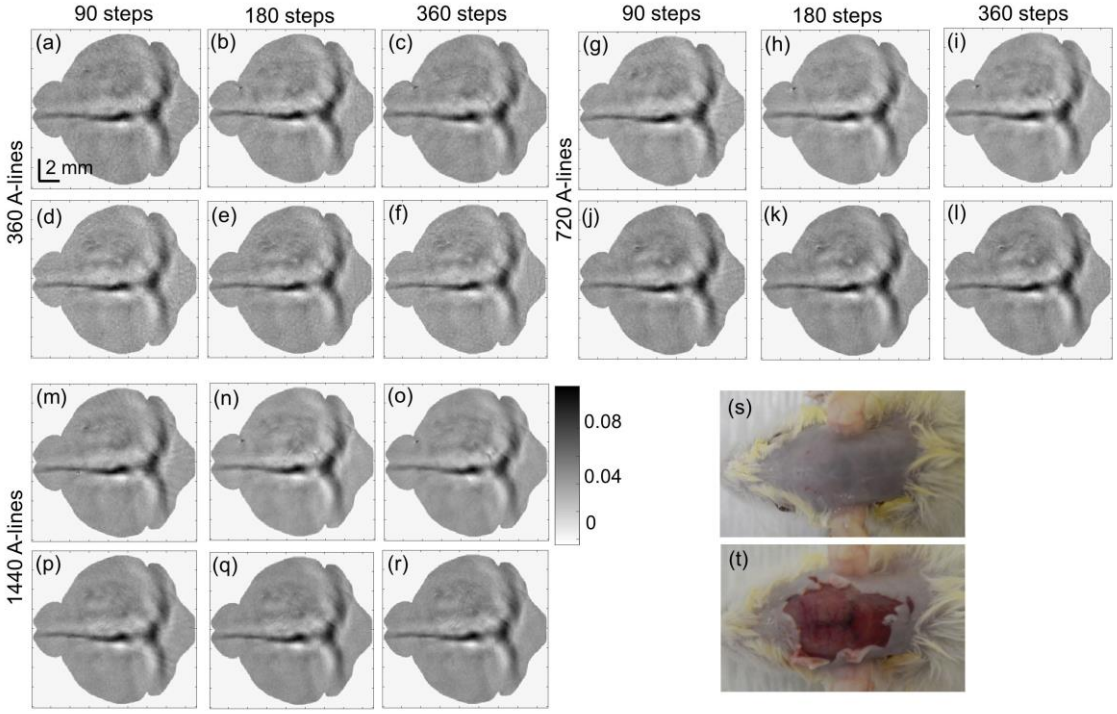

Fig. 5. Comparison of *in vivo* brain PAT images of female rat for (a-c, g-i, m-o) stop-and-go and (d-f, j-l, p-r) continuous scanning methods. (a-f) 360, (g-i) 720, and (m-r)1440 A-lines were collected and were averaged in (a, d, g, j, m, p) 90, (b, e, h, k, n, q) 180, and (c, f, i, l, o, r) 360 A-lines corresponding to the number of steps taken in stop-and-go scans. Scale bar is shown in (a). Photographs of rat brain (s) before and (t) after skin removal are shown.

Table I: SNR (dB) for phantom imaging. The SNR values are for point source imaging (Nd:YAG based PAT) and triangle phantom imaging (PLD-PAT)

Laser (PRR)	**A-lines collected**	**90 A-lines reconstructed**		**180 A-lines reconstructed**		**360 A-lines reconstructed**	
		Stop-and-go	Continuous	Stop-and-go	Continuous	Stop-and-go	Continuous
Nd:YAG (10 Hz)	180	23.9	23.4	24.3	24.1	N/A	N/A
	360	24.9	24.4	25.1	24.9	27.2	26.6
	720	25.5	26.4	27.6	27.7	29.2	30.5
	1440	26.2	26.6	29.3	28.7	33.2	33.3
	2880	27.6	26.9	28.8	28.3	36.3	36.1
PLD (7 kHz)	63000	16.5	17.7	25.8	26.7	34.5	34.4
	126000	16.6	17.2	24.1	25.3	35.5	35.6

Table II: SNR (dB) for *in vivo* rat brain imaging

Laser (PRR)	**A-lines collected**	**90 A-lines reconstructed**		**180 A-lines reconstructed**		**360 A-lines reconstructed**	
		Stop-and-go	Continuous	Stop-and-go	Continuous	Stop-and-go	Continuous
Nd:YAG (10 Hz)	360	15.9	15.9	18.8	17.8	19.2	18.2
	720	17.6	17.2	21.2	20.4	21.8	20.5
	1440	18.2	18.6	24.2	22.6	24.5	23.3
PLD (7 kHz)	126000	17.8	17.1	21.4	20.6	22.2	20.7

For rat brain imaged using PLD-PAT system, velocity of motor for continuous scans was fixed at 20°/second, i.e., it completed one rotation in 18 seconds collecting 126000 A-lines. For stop-and-go scans, the motor completed one rotation in 90, 180, and 360 steps with a maximum velocity of ~7°/second between two stops. 126000 A-lines were collected by collecting 1400, 700, and 350 A-lines per step, respectively. Images acquired by moving UST in steps of 1°, 2°, and 4° (stop-and-go scans) are shown in Figs. 6(a-c), respectively. Figs. 6(d-f) were acquired by collecting A-lines continuously, but finally averaging them into 90, 180, and 360 A-lines, respectively, before reconstruction. Photographs of rat

taken before [Fig. 6(g)] and after [Fig. 6(h)] skin removal are shown to verify the acquired images.

SNR of these images are also given in Table II. When the number of A-lines reconstructed was increased from 90 to 360, a ~27% increase in SNR was observed for stop-and-go scan and ~21% increase for continuous scan. However, for the same number of A-lines reconstructed, ~7% decrease in SNR was observed in continuous scans as compared to stop-and-go scans. For most cases, this decrease is not prominent and therefore can be considered inconsequential. Thus, the results obtained were similar to those obtained using Nd:YAG based PAT system. The increase in speed of PLD based system was compensated by the increase in number of A-lines collected due to higher PRR. Therefore, although the transducer was moving at a higher speed, the blur due to continuous scans was insignificant.

Another parameter to compare image quality is resolution of the system. Images of triangle phantom were used for the same because the diameter of horsehair used was less than the expected resolution of the system. Line profiles along different cross sections of horsehair (i.e., perpendicular to edges of triangle) were plotted and fitted to a Gaussian curve. Full width at half maximum values of this curve provided the resolution. Resolution along different line profiles were averaged for more accurate measurements. Table III shows the calculated resolution for different types of scans. An improvement in resolution of stop-and-go scans as compared to continuous scans, can be observed in the table. The improvement is more prominent (4-6%) when 90 A-lines are reconstructed and negligible (1-3%) when 360 A-lines are reconstructed. Furthermore, for continuous scans, the resolution improves when more number of A-lines is reconstructed. No such trend is however visible in stop-and-go scans.

Table III: Resolution (μm) for different scans of PLD-PAT system. Scan1: stop-and-go scan, Scan2: continuous scan

A-lines collected	90 A-lines reconstructed		180 A-lines reconstructed		360 A-lines reconstructed	
	Scan1	Scan2	Scan1	Scan2	Scan1	Scan2
63000	343	363	348	357	345	355
126000	339	360	339	353	352	351

B. *Scan time and laser exposure*

As shown above, scan time for stop-and-go scans will be much higher than continuous scans if maximum speed and acceleration are kept constant. For continuous scans, the maximum speed is related to the number of A-lines collected and therefore the speed cannot be manipulated. This is not the case with stop-and-go scans, where the speed is limited by the motor and the vibrations it can cause and not by the number of A-lines. Before performing the experiments, the velocity and acceleration of stepper motor were optimized such that scan time was the least and vibrations minimal.

An increase in scan time not only prevents real-time imaging, but also results in higher laser exposure. In continuous scan, the sample is exposed to laser only during imaging, when it is necessary. In contrast, in stop-and-go scans, apart from imaging time, the sample is exposed to laser while the transducer is moving around the sample. This is a concern especially for biomedical imaging. Table IV shows the scan time and the number of laser pulses the sample got exposed to. From Table IV it can be observed that continuous scans were ~4 times faster than stop-and-go scans when lesser number of A-lines (180 and 360) were collected and ~1.5 times faster when higher number of A-lines were collected, for Nd:YAG-PAT system. Further, decrease in acquisition time for continuous scans as compared to stop-and-go scans was 7-12 folds for PLD-PAT system, when same number of A-lines were acquired in both. This resulted in a significant decrease in laser exposure of the sample particularly for PLD-PAT.

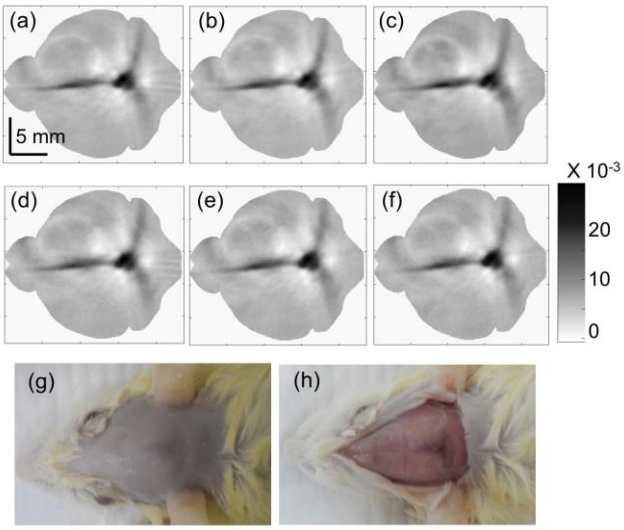

Fig. 6. Experimental results of *in vivo* brain images of female rat using PLD-PAT system. Images were acquired using (a-c) stop-and-go and (d-f) continuous scanning methods. 12600 A-lines were collected by moving the motor in (a) 90 steps, (b) 180 steps, (c) 360 steps, and (d-f) continuously for 18 sec. The collected A-lines were averaged into (a, d) 90 A-lines, (b, e) 180 A-lines, and (c, f) 360 A lines before reconstruction. Scale bar is same for all images as shown in (a). Photographs of brain are shown (g) before and (h) after skin removal.

Another observation made from Table IV was that for the same number of A-lines collected, the data acquisition time increased by only ~10% when the number of steps was increased, in case of Nd:YAG based PAT system. As can be seen from (1), on increasing the number of steps, the scan time should increase by a factor of number of steps multiplied by (ω/α), i.e., velocity divided by acceleration. For our experiments, the acceleration was kept much larger than velocity, making the ratio of velocity and acceleration almost negligible as compared to the rest of the equation. However, this factor becomes prominent when the total scan time is less, like in PLD based PAT system, wherein the scan time increases by ~60% when the number of steps is increased. It should also be noted that the experimental scan time was more than the practical scan time for all the experiments. This was

due to vibrations of the motor after moving each step. Motion of motor was optimized such that after each step it needs to wait for a few milliseconds before starting signal collection.

It can therefore be concluded that in terms of scan time and laser exposure, continuous scans have an advantage over stop-and-go scans. This advantage becomes more prominent while using high repetition rate lasers like LED/PLD. In case of low repetition rate laser (like Nd:YAG) the improvement of scan time is apparent when less number of A-lines is collected.

Table IV: Comparison of scan time and laser exposure (number of pulses the sample got exposed to) for continuous and stop-and-go scans.

Laser	**Stop-and-go (90 steps)**		**Stop-and-go (180 steps)**		**Stop-and-go (360 steps)**		**Continuous Scan**	
	Scan time (A-lines)	Laser pulses	Scan time (A-lines)	Laser pulses	Scan time (A-lines)	Laser pulses	Scan time (A-lines)	Laser pulses
Nd:YAG (10 Hz)	80 s (180)	800	95 s (180)	950	N/A	N/A	18 s (180)	180
	98 s (360)	980	108 s (360)	1080	109 s (360)	1090	36 s (360)	360
	135 s (720)	1350	147 s (720)	1470	145 s (720)	1450	72 s (720)	720
	210 s (1440)	2100	217 s (1440)	2170	217 s (1440)	2170	144 s (1440)	1440
	355 s (2880)	3550	362 s (2880)	3620	364 s (2880)	3640	288 s (2880)	2880
PLD (7 kHz)	78 s (63000)	546000	90 s (63000)	630000	125 s (63000)	875000	9 s (63000)	63000
	87 s (126000)	609000	99 s (126000)	693000	132 s (126000)	924000	18 s (126000)	126000

IV. Conclusion

In this work, we have compared the two scanning methods that are being used for PAT/PACT imaging systems. We have provided experimental data of phantoms as well as *in vivo* rat brain images for the comparison. The results indicate that various factors should be considered while choosing the type of scan. For smaller samples (in the range of 10-30 mm), it is better to use continuous scans, as for these samples the image quality remains quite similar for both the types of scans, and the data acquisition time is much less for continuous scans. The results also indicate that while collecting same number of A-lines for stop-and-go scans, it was better to complete the rotation in more number of steps. Increasing the number of steps improved the image quality, with only a slight increase in data acquisition time, specially for lasers with low PRR. Another factor influencing the choice of scanning method should be the PRR of the laser. Performing stop-and-go scans for lasers with high PRR exposes the samples to more number of laser pulses, which may be a safety concern. Hence, we conclude that continuous scans should be preferred over stop-and-go scans, especially during biomedical imaging of small objects using lasers with high PRR.

References

[1] L. Li, L. Zhu, C. Ma, L. Lin, J. Yao, L. Wang, *et al.*, "Single-impulse panoramic photoacoustic computed tomography of small-animal whole-body dynamics at high spatiotemporal resolution," *Nature Biomedical Engineering*, vol. 1, p. 0071, 2017.

[2] P. K. Upputuri and M. Pramanik, "Recent advances toward preclinical and clinical translation of photoacoustic tomography: a review," *Journal of Biomedical Optics*, vol. 22, p. 041006, 2017.

[3] S. Hu, "Listening to the Brain With Photoacoustics," *IEEE Journal of Selected Topics in Quantum Electronics*, vol. 22, p. 6800610, 2016.

[4] L. V. Wang and J. Yao, "A practical guide to photoacoustic tomography in the life sciences," *Nature Methods*, vol. 13, pp. 627-38, 2016.

[5] J. Xia and L. V.Wang, "Small-Animal Whole-Body Photoacoustic Tomography: A Review," *IEEE Transactions on Biomedical Engineering*, vol. 61, pp. 1380-89, 2014.

[6] S. Zackrisson, S. van de Ven, and S. Gambhir, "Light in and sound out: emerging translational strategies for photoacoustic imaging," *Cancer research*, vol. 74, pp. 979-1004, 2014.

[7] L. V. Wang and S. Hu, "Photoacoustic Tomography: In Vivo Imaging from Organelles to Organs," *Science*, vol. 335, pp. 1458-1462, 2012.

[8] P. Beard, "Biomedical photoacoustic imaging," *Interface Focus*, vol. 1, pp. 602-31, 2011.

[9] L. V. Wang, "Multiscale photoacoustic microscopy and computed tomography," *Nature Photonics*, vol. 3, pp. 503-509, 2009.

[10] J. J. Yao, J. Xia, K. I. Maslov, M. Nasiriavanaki, V. Tsytsarev, A. V. Demchenko, *et al.*, "Noninvasive photoacoustic computed tomography of mouse brain metabolism in vivo," *Neuroimage*, vol. 64, pp. 257-266, 2013.

[11] X. D. Wang, Y. J. Pang, G. Ku, G. Stoica, and L. V. Wang, "Three-dimensional laser-induced photoacoustic tomography of mouse brain with the skin and skull intact," *Optics Letters*, vol. 28, pp. 1739-1741, 2003.

[12] K. Sivasubramanian, V. Periyasamy, and M. Pramanik, "Non-invasive sentinel lymph node mapping and needle guidance using clinical handheld photoacoustic imaging system in small animal," *Journal of Biophotonics*, vol. 11, p. e201700061, 2018.

[13] D. Pan, M. Pramanik, A. Senpan, S. Ghosh, S. A. Wickline, L. V. Wang, *et al.*, "Near infrared photoacoustic detection of sentinel lymph nodes with gold nanobeacons," *Biomaterials*, vol. 31, pp. 4088-93, 2010.

[14] W. Xia, D. Piras, M. K. A. Singh, J. C. G. van Hespen, T. G. van Leeuwen, W. Steenbergen, *et al.*, "Design and evaluation of a laboratory prototype system for 3D photoacoustic full breast tomography," *Biomedical Optics Express*, vol. 4, pp. 2555-69, 2013.

[15] D. Piras, W. Steenbergen, T. G. van Leeuwen, and S. Manohar, "Photoacoustic Imaging of the Breast Using the Twente Photoacoustic Mammoscope: Present Status and Future Perspectives," *IEEE Journal of Selected Topics in Quantum Electronics*, vol. 16, pp. 730-739, 2010.

[16] M. Pramanik, G. Ku, C. Li, and L. V. Wang, "Design and evaluation of a novel breast cancer detection system combining both thermoacoustic (TA) and photoacoustic (PA) tomography," *Medical Physics*, vol. 35, pp. 2218-23, 2008.

[17] X. Wang, X. Xie, G. Ku, L. V. Wang, and G. Stoica, "Noninvasive imaging of hemoglobin concentration and oxygenation in the rat brain using high-resolution photoacoustic tomography," *Journal of Biomedical Optics*, vol. 11, p. 024015, 2006.

[18] J. Yao, J. Xia, and L. V. Wang, "Multiscale Functional and Molecular Photoacoustic Tomography," *Ultrason Imaging*, vol. 38, pp. 44-62, 2016.

[19] C. Li and L. V. Wang, "Photoacoustic tomography and sensing in biomedicine," *Physics in Medicine and Biology*, vol. 54, pp. R59-97, 2009.

[20] L. V. Wang, "Tutorial on Photoacoustic Microscopy and Computed Tomography," *IEEE Journal of selected topics in Quantum electronics*, vol. 14, pp. 171-179, 2008.

[21] S. Gutta, M. Bhatt, S. K. Kalva, M. Pramanik, and P. K. Yalavarthy, "Modeling errors compensation with total least squares for limited data photoacoustic tomography," *IEEE Journal of Selected Topics in Quantum Electronics*, 2019 (In Press).

[22] S. K. Kalva and M. Pramanik, "Experimental validation of tangential resolution improvement in photoacoustic tomography using a modified delay-and-sum reconstruction algorithm," *Journal of Biomedical Optics*, vol. 21, p. 086011, 2016.
[23] M. Pramanik, "Improving tangential resolution with a modified delay-and-sum reconstruction algorithm in photoacoustic and thermoacoustic tomography," *Journal of the Optical Society of America A*, vol. 31, pp. 621-7, 2014.
[24] C. Lutzweiler, X. L. Dean-Ben, and D. Razansky, "Expediting model-based optoacoustic reconstructions with tomographic symmetries," *Medical Physics*, vol. 41, p. 013302, 2014.
[25] J. Prakash, A. S. Raju, C. B. Shaw, M. Pramanik, and P. K. Yalavarthy, "Basis pursuit deconvolution for improving model-based reconstructed images in photoacoustic tomography," *Biomedical Optics Express*, vol. 5, pp. 1363-77, 2014.
[26] C. Huang, K. Wang, L. Nie, L. V. Wang, and M. A. Anastasio, "Full-Wave Iterative Image Reconstruction in Photoacoustic Tomography with Acoustically Inhomogeneous Media," *IEEE Transactions on Medical Imaging*, vol. 32, pp. 1097-1110, 2013.
[27] S. K. Kalva and M. Pramanik, "Use of acoustic reflector to make compact photoacoustic tomography system," *Journal of Biomedical Optics*, vol. 22, p. 026009, 2017.
[28] P. Hai, Y. Zhou, R. Zhang, J. Ma, Y. Li, J.-Y. Shao, *et al.*, "Label-free high-throughput detection and quantification of circulating melanoma tumor cell clusters by linear-array-based photoacoustic tomography," *Journal of Biomedical Optics*, vol. 22, p. 041004, 2017.
[29] K. Sivasubramanian and M. Pramanik, "High frame rate photoacoustic imaging at 7000 frames per second using clinical ultrasound system," *Biomedical Optics Express*, vol. 7, pp. 312-323, 2016.
[30] W. Shu, M. Ai, T. Salcudean, R. Rohling, P. Abolmaesumi, and S. Tang, "Broadening the detection view of 2D photoacoustic tomography using two linear array transducers," *Optics Express*, vol. 24, pp. 12755-68, 2016.
[31] A. Buehler, X. L. Deán-Ben, J. Claussen, V. Ntziachristos, and D. Razansky, "Three-dimensional optoacoustic tomography at video rate," *Optics Express*, vol. 20, pp. 22712-19, 2012.
[32] C. Li, A. Aguirre, J. Gamelin, A. Maurudis, Q. Zhu, and L. V. Wang, "Real-time photoacoustic tomography of cortical hemodynamics in small animals," *Journal of Biomedical Optics*, vol. 15, p. 010509, 2010.
[33] X. L. Dean-Ben and D. Razansky, "Portable spherical array probe for volumetric real-time optoacoustic imaging at centimeter-scale depths," *Optics Express*, vol. 21, pp. 28062-71, 2013.
[34] P. K. Upputuri and M. Pramanik, "Dynamic in vivo imaging of small animal brain using pulsed laser diode-based photoacoustic tomography system," *Journal of Biomedical Optics*, vol. 22, p. 090501, 2017.
[35] Z. Deng, W. Li, and C. Li, "Slip-ring-based multi-transducer photoacoustic tomography system," *Optics Letters*, vol. 41, pp. 2859-62, 2016.
[36] R. Cheng, J. Shao, X. Gao, C. Tao, J. Ge, and X. Liu, "Noninvasive Assessment of Early Dental Lesion Using a Dual-Contrast Photoacoustic Tomography," *Scientific Reports*, vol. 6, p. 21798, 2016.
[37] P. K. Upputuri and M. Pramanik, "Performance characterization of low-cost, high-speed, portable pulsed laser diode photoacoustic tomography (PLD-PAT) system," *Biomedical Optics Express*, vol. 6, pp. 4118-29, 2015.
[38] G. Ku, X. Wang, G. Stoica, and L. V. Wang, "Multiple-bandwidth photoacoustic tomography," *Physics in Medicine and Biology*, vol. 49, pp. 1329-38, 2004.
[39] "American National Standard for Safe Use of Lasers ANSI Z136.1-2007 (American National Standards Institute, Inc., New York, NY, 2007)," ed.
[40] R. Ma, A. Taruttis, V. Ntziachristos, and D. Razansky, "Multispectral optoacoustic tomography (MSOT) scanner for whole-body small animal imaging," *Optics Express*, vol. 17, pp. 21414-26, 2009.
[41] M. Toi, Y. Asao, Y. Matsumoto, H. Sekiguchi, A. Yoshikawa, M. Takada, *et al.*, "Visualization of tumor-related blood vessels in human breast by photoacoustic imaging system with a hemispherical detector array," *Scientific Reports*, vol. 7, 2017.
[42] M. Heijblom, D. Piras, M. Brinkhuis, J. C. van Hespen, F. M. van den Engh, M. van der Schaaf, *et al.*, "Photoacoustic image patterns of breast carcinoma and comparisons with Magnetic Resonance Imaging and vascular stained histopathology," *Scientific Reports*, vol. 5, p. 11778, 2015.

Arunima Sharma received her integrated dual degree with bachelor's in bioengineering and master's in biomedical technology from Indian Institute of Technology (Banaras Hindu University), Varanasi, India, in 2016. She is currently pursuing her PhD degree in School of Chemical and Biomedical Engineering, Nanyang Technological University, Singapore. Her current research interests include development of photoacoustic imaging systems, and application of photoacoustics in biomedical imaging.

Sandeep Kumar Kalva received his master's degree in biomedical engineering from the Indian Institute of Technology (IIT), Hyderabad, India, in 2015. He is currently a PhD student in the School of Chemical and Biomedical Engineering, Nanyang Technological University, Singapore. His research area is on functional photoacoustic imaging for various clinical applications.

Manojit Pramanik received his PhD in biomedical engineering from Washington University in St. Louis, Missouri, USA. Currently, he is an assistant professor of the School of Chemical and Biomedical Engineering, Nanyang Technological University, Singapore. His research interests include the development of photoacoustic/thermoacoustic imaging systems, image reconstruction methods, clinical application areas such as breast cancer imaging, molecular imaging, contrast agent development, and Monte Carlo simulation of light propagation in biological tissue.